IEEE Access
Multidisciplinary : Rapid Review : Open Access Journal

Received July 11, 2019, accepted August 6, 2019, date of publication August 12, 2019, date of current version August 22, 2019.

Digital Object Identifier 10.1109/ACCESS.2019.2934494

A Balanced Quad-Band BPF With Independently Controllable Frequencies and High Selectivity

FENG WEI, (Member, IEEE), HAO JIE YUE, XIAO HANG ZHANG, AND XIAO-WEI SHI, (Senior Member, IEEE)

National Key Laboratory of Antennas and Microwave Technology, Collaborative Innovation Center of Information Sensing and Understanding, School of Electrical Engineering, Xidian University, Xi'an 710071, China

Corresponding author: Feng Wei (fwei@mail.xidian.edu.cn)

This work was supported in part by the Fundamental Research Funds for the Central Universities under Grant JB180204, and in part by the State Key Laboratory of Metamaterial Electromagnetic Modulation Technology under Grant GYL08-1444.

ABSTRACT A balanced microstrip quad-band bandpass filter (BPF) with independently controllable frequencies, controllable fractional bandwidths (FBWs) and high selectivity is designed in this paper. The proposed BPF is achieved by employing two pairs of folded asymmetric stub-loaded resonators (FASLRs) and balanced microstrip/slotline transition structures (MSTSs). The center frequencies of the four differential-mode (DM) passbands can be controlled independently by changing the electrical lengths of each FASLR. A novel interdigital coupled line is firstly proposed to enhance source-load coupling further, which contributes to a higher selectivity. Meanwhile, the DM passbands are independent of the CM responses, which significantly simplifies the design procedure. In addition, eight transmission zeros (TZs) are generated to improve the selectivity of the four passbands obviously. The measured results of the fabricated balanced BPF centered at 2.48/3.45/5.17/5.78 GHz agree well with the simulated ones, which validates the proposed design method well.

INDEX TERMS Asymmetric stub-loaded resonators, balanced BPF, microstrip/slotline transition structures (MSTSs), interdigital coupled line, quad-band.

I. INTRODUCTION

With the continuous progress of wireless communication technology, such as global positioning system (GPS), wireless local area network (WLAN), worldwide interoperability for microwave access (WiMAX) and mobile cellular systems, multi-band technology has become a research hotspot in recent years [1]–[6]. On the other hand, balanced circuits have attracted substantial attention and have been more and more utilized because of the high immunity to the environmental noise, interference and crosstalk between different elements, compared with the single-end counterparts. To increase the capacity of wireless systems, many researches are focusing on balanced dual/tri-band bandpass filters (BPFs) [7]–[10]. However, to our best knowledge, only one balanced quad-band BPF was reported in the past years [11]. The proposed balanced quad-band BPF shows controllable frequencies and intrinsic common-mode (CM) rejection. However, the measured insertion losses at high frequencies are large and the selectivity needs to be improved further.

The associate editor coordinating the review of this article and approving it for publication was Kai-Da Xu.

In this paper, a balanced quad-band BPF with independently controllable frequencies, controllable fractional bandwidths (FBWs) and eight transmission zeros (TZs) is designed. The proposed BPF is fed by a pair of U-type balanced microstrip-slotline transition structures (MSTS), which achieves an independent common-mode (CM) response with a larger bandwidth and a superior suppression. Two pairs of folded asymmetric stub-loaded resonators (FASLRs) are introduced to generate four differential-mode (DM) passbands. Meanwhile, a novel capacitive-ended interdigital coupled line is firstly proposed and employed between the two FASLRs to enhance source-load coupling further. In addition, eight TZs are generated to improve the selectivity greatly. Based on the above structure, a balanced quad-band BPF is designed and fabricated. The simulation and measurement results are found to be in a good agreement.

II. BALANCED QUAD-BAND BPFS

Fig. 1 (a) illustrates the configuration of the proposed balanced quad-band BPF, which consists of a pair of balanced MSTSs, two sets of FASLRs and a novel capacitive-ended

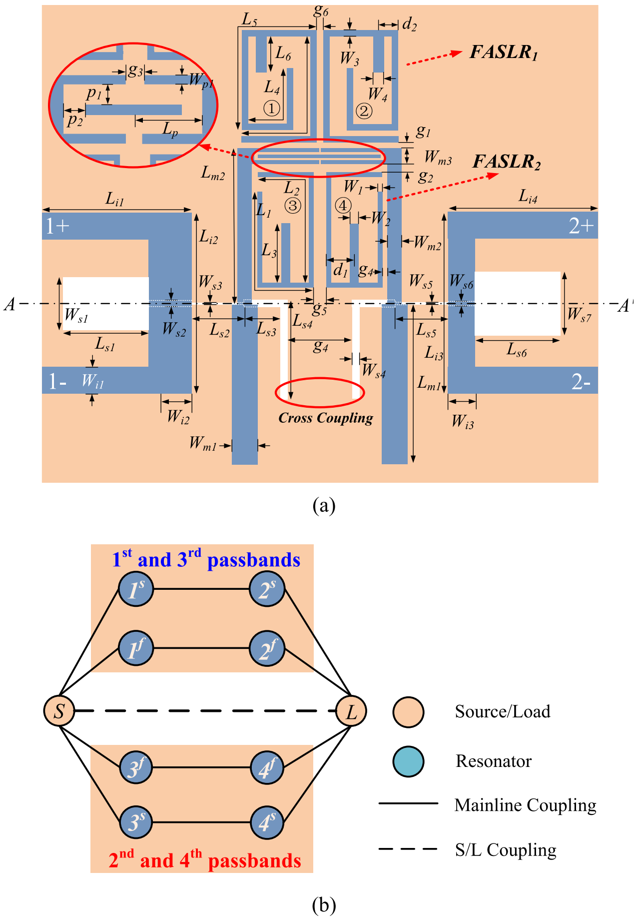

FIGURE 1. (a) Configuration and (b) Coupling scheme of the DM response of the proposed balanced quad-band BPF.

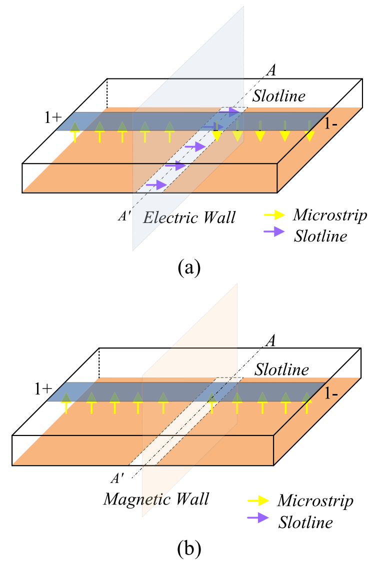

FIGURE 2. 2 Electric field in balanced MSTS structure under (a) DM and (b) CM operation.

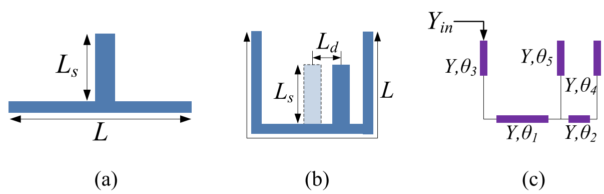

FIGURE 3. Configuration of (a) CSLR, (b)FASLR and (c) Equivalent circuit of FASLR.

interdigital coupled line loaded at the middle of two step-impedance microstrip line. Each balanced MSTS comprises a U-type microstrip feedline and a stepped-impedance slotline resonator. The stepped-impedance slotline resonator is etched on the bottom layer of the substrate and is crossed with the U-type microstrip line on the top layer of the substrate vertically. Meanwhile, the slotline resonator extends about a quarter of wavelength beyond the U-type microstrip feedline to couple with each other. What's more, two pairs of symmetrical FASLRs are employed on both sides of capacitive-ended interdigital coupled line on the top layer, respectively, which generate the four DM passbands collectively. Fig. 1 (b) displays the coupling scheme of the DM response of the balanced quad-band BPF described by four paralleled coupling paths, where 1^f represents the fundamental resonant frequency of resonator ① and 1^s represents the first spurious frequencies of resonator ① (the same below).

A. INTRINSIC CM SUPPRESSION

Fig. 2 shows the electric field in balanced MSTSs under DM and CM operation, respectively, where *A-A'* is the symmetry plane of the transition structure. When a DM excitation is applied, a virtual electrical wall can be obtained at the symmetric plane *A-A'*. Through strong magnetic coupling, the DM signals along the U-type microstrip line can be converted successfully into the slotline mode and be transferred to the next structure. Under CM signal excitation, *A-A'* is equivalent to a magnetic wall, so the mode in the slotline can't be excited, and then the CM signal is blocked. Since the suppression characteristic of balanced MSTS on CM signals is determined by its own boundary conditions and independent of frequency, its suppression is wideband and natural [12]. Thus, only the DM performance is left to be focused in this paper, which significantly simplifies the design procedure.

B. DM RESPONSE

Traditional microstrip center stub-loaded resonators (CSLRs) consists of a half wavelength resonator and an open stub loaded at the midpoint. Differently, asymmetric stub-loaded resonators (ASLR) introduces an additional resonance mode because the position of center-loaded stub is free. In order to achieve miniaturization, the stubs on both sides of ASLR are folded inward to form FASLR. Fig. 3(a) and 3(b) gives the schematic diagram of CSLR and the FASLR, in which the length of the folded half-wavelength resonator is L and the loaded stub is L_s. The displacement of the asymmetric stub from the center is L_d. Equivalent circuit of FASLR is given in Fig. 3(c). The characteristic admittance of the resonator is Y, the electrical length of the half-wavelength

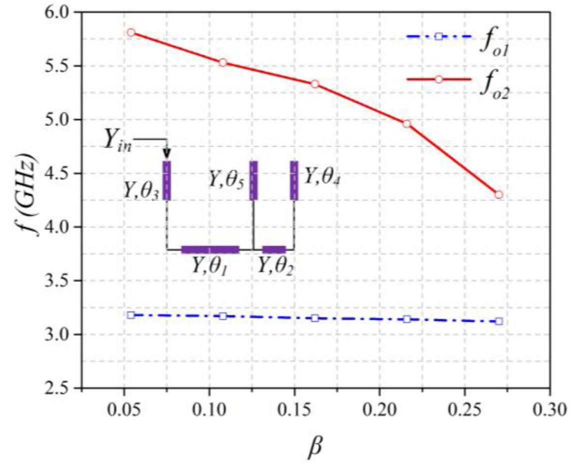

FIGURE 4. Value of f_{o1} and f_{o2} against β.

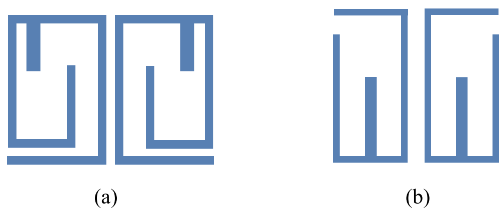

FIGURE 5. Configuration of (a) $FASLR_1$ and (b)$FASLR_2$.

resonator is θ_T ($\theta_T = \theta_1 + \theta_2 + \theta_3 + \theta_4$), and the electrical length of the loaded stub is θ_5, where $\theta_1 + \theta_3 \neq \theta_2 + \theta_4$. Now α and β are defined as follows:

$$\alpha = \frac{\theta_2 + \theta_4}{\theta_1 + \theta_2 + \theta_3 + \theta_4} = \frac{\theta_2 + \theta_4}{\theta_T} \tag{1}$$

$$\beta = \frac{\theta_5}{\theta_1 + \theta_2 + \theta_3 + \theta_4} = \frac{\theta_5}{\theta_T} \tag{2}$$

where α is defined in accordance with the ratio of the shorter section to total length of the half-wavelength resonator, and β is determined as the radio of loaded stub to the total length of the half-wavelength resonator. According to the transmission line theory, the fundamental frequency and the first spurious frequency of FASLR are determined by appropriately choosing the electrical length ratio α and β [13]. As shown in Fig. 4, f_{o2} (the first spurious frequency of FASLR) varies significantly with β while f_{o1} (fundamental frequency of FASLR) remains almost the same. In this paper, $FASLR_1$ (FASLR above the interdigital coupled line) is folded up into six sections while $FASLR_2$ (FASLR below the interdigital coupled line) is folded up into four sections to achieve immensely miniaturization, as shown in Fig. 5. Therefore, the desired frequencies can be obtained by changing the electrical length of $FASLR_1$ and $FASLR_2$, respectively. Fig. 6 presents the transmission response curve of FASLR, three resonant frequencies are generated within the given frequency range. They are fundamental resonant frequency, the first spurious frequency and the second spurious frequency, respectively.

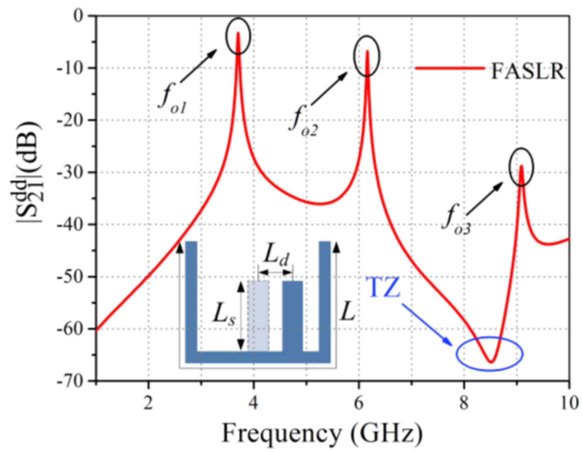

FIGURE 6. Transmission response curve of FASLR.

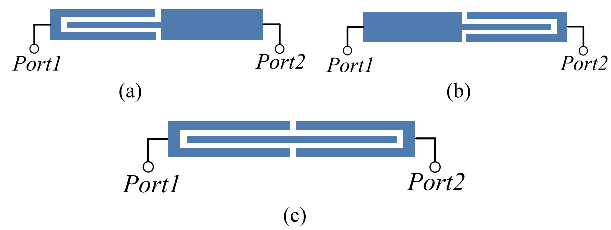

FIGURE 7. Interdigital coupled line with capacitive-end coupling on the (a) left, (b) right and (c) the proposed capacitive-ended interdigital coupled line.

It can be seen that one TZ is generated on the right side of the first spurious frequency, which contributes to higher selectivity at the upper frequency of the proposed balanced BPF.

C. CAPACITIVE-ENDED INTERDIGITAL COUPLED LINE

Fig. 7 (a) and (b) shows the conventional interdigital coupled lines, which are widely used in wideband bandpass filters because they can achieve tight coupling and enhance the out-of-band performance without affecting in-band characteristics [14]. In this paper, a novel interdigital coupled line is firstly proposed by the combination of the interdigital coupled lines on both sides, as shown in Fig. 7 (c). Compared with the end-coupling, interdigital coupled line adds multiple transmission paths by etching an interdigital slot on the feed-line to realize parallel coupling between the source and load. Therefore, multi-path transmissions are achieved to increase the number of transmission zeros and improve out-of-band suppression. In addition, the novel interdigital coupled line is proposed by the combination of the interdigital coupled lines on both sides, which further improves out-of-band suppression since transmission paths double. In this paper, higher selectivity is obtained by employing the proposed interdigital coupled line between $FASLR_1$ and $FASLR_2$. Fig. 8 (a) shows the S-parameters of no interdigital coupled line, conventional interdigital coupled line and the proposed one, respectively.

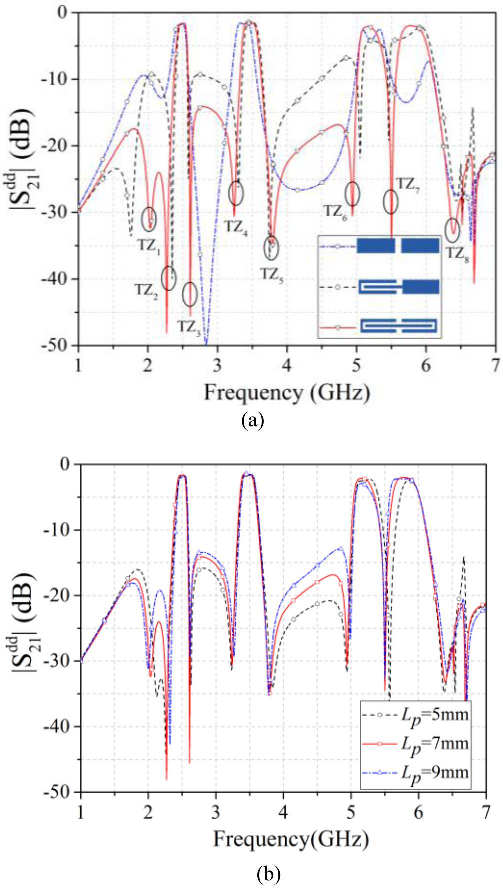

FIGURE 8. Comparison of S-parameters with (a) different type of interdigital coupled lines and (b) half length of the proposed interdigital coupled line.

It is observed that that the proposed interdigital coupled line generates four TZs, including TZ_2, TZ_4, TZ_5 and TZ_6. Meanwhile, evident out-of-band suppression improvement between the four DM passbands is obtained. Fig. 8 (b) shows the S-parameters versus different L_p (half physical length of the proposed interdigital coupled line), which indicates that a short interdigital coupled line can achieve a better out-of-band suppression.

D. BALANCED BPF DESIGN

Four DM passbands are generated by employing $FASLR_1$ and$FASLR_2$. Since the characteristics of FASLR have been analyzed above that the resonant frequency of FASLR is determined by appropriately choosing the electrical length ratio α and β. Now α_1 is defined in accordance with the ratio of the shorter section to total length of the half-wavelength resonator of $FASLR_1$ (the same as α_2). β_1 is determined as the radio of loaded stub to the total length of the half-wavelength resonator of $FASLR_1$ (the same as β_2). As shown in Fig. 9, f_1 (center frequency of the first DM passband, the same below) is determined by α_1 while f_3 can be only controlled by the length of open-stub β_1. Similarly, f_2 is determined by α_2 while f_4 can only be controlled by the length of open-stub β_2. Therefore, the four DM center

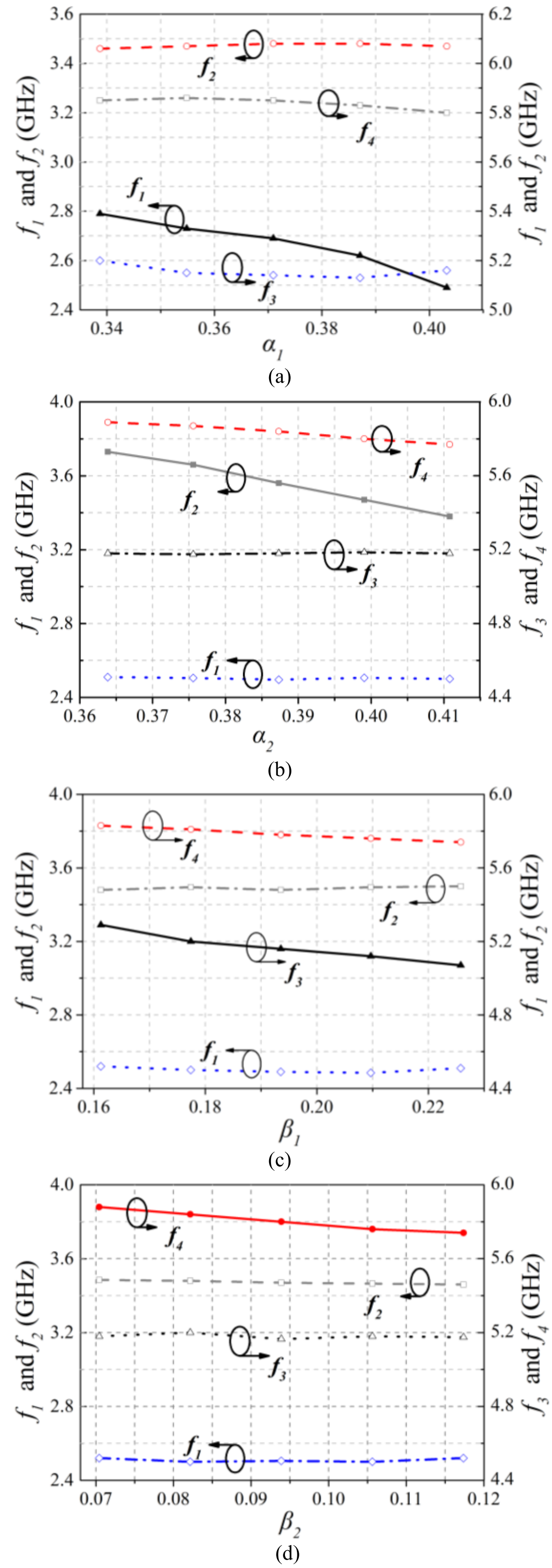

FIGURE 9. Variation of the four DM passbands with different dimensions (a) α_1, (b) α_2, (c) β_1 and (d) β_1.

frequencies can be controlled independently by adjusting the electrical lengths of FASLRs. In addition, it is noteworthy that $FASLR_1$ is only fed by the capacitive-ended interdigital

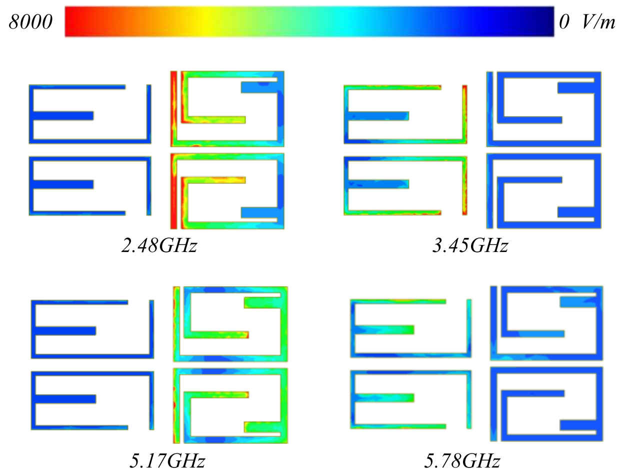

FIGURE 10. Current distributions of the two resonators at 2.48 GHz, 3.45 GHz, 5.17 GHz and 5.78 GHz.

coupled line while $FASLR_2$ is fed by the capacitive-ended interdigital coupled line and L-shaped stepped-impedance microstrip line simultaneously. Fig. 10 displays the current distributions of the resonators at 2.48 GHz, 3.45 GHz, 5.17 GHz and 5.78 GHz, respectively, which was simulated in HFSS 13.0. Though the distribution plots, it can be found that the current in two FSLRs at 2.48 GHz and 3.45 GHz is much stronger in each folded half wavelength resonators while that at 5.17 GHz and 5.78 GHz distributes throughout the overall resonators, including the open stubs. The transmission of EM waves and the generation of the four DM passbands can be further verified. Since the coupling strength is related to coupling spacing, the coupling strength of the two pairs of resonators can be controlled by g_1 (gap between L-shaped microstrip line and $FASLR_1$) and g_2 (gap between L-shaped microstrip line and $FASLR_2$). Therefore, FBW_1 (fractional bandwidth of the first passbands, the same below) and FBW_3 can be controlled simultaneously by parameter g_1 while FBW_2 and FBW_4 can be controlled simultaneously by parameter g_1. In addition, eight TZs are generated around the four DM passbands to improve the selectivity of the BPF significantly. The proposed interdigital coupled line generates four TZs by adding multiple transmission paths as analyzed above, including TZ_2, TZ_4, TZ_5 and TZ_6. Except for the above-mentioned four TZs, TZ_1 is generated by the cross coupling between the two slotline resonators. And the position of TZ_1 is determined by the coupling strength between the two L-shaped slotline resonators. TZ_3 is achieved by the source-load coupling between the L-shaped step-impedance microstrip lines. What's more, TZ_7 and TZ_8 are realized because of the intrinsic characteristics of the FASLRs, as analyzed above. The position of TZ_7 and TZ_8 can be controlled by the length of loaded stub of each FASLR.

III. EXPERIMENTAL RESULTS AND DISCUSSION

The substrate used in this BPF is Rogers 5880 with a thickness of 0.8 mm and a relative permittivity of 2.2.

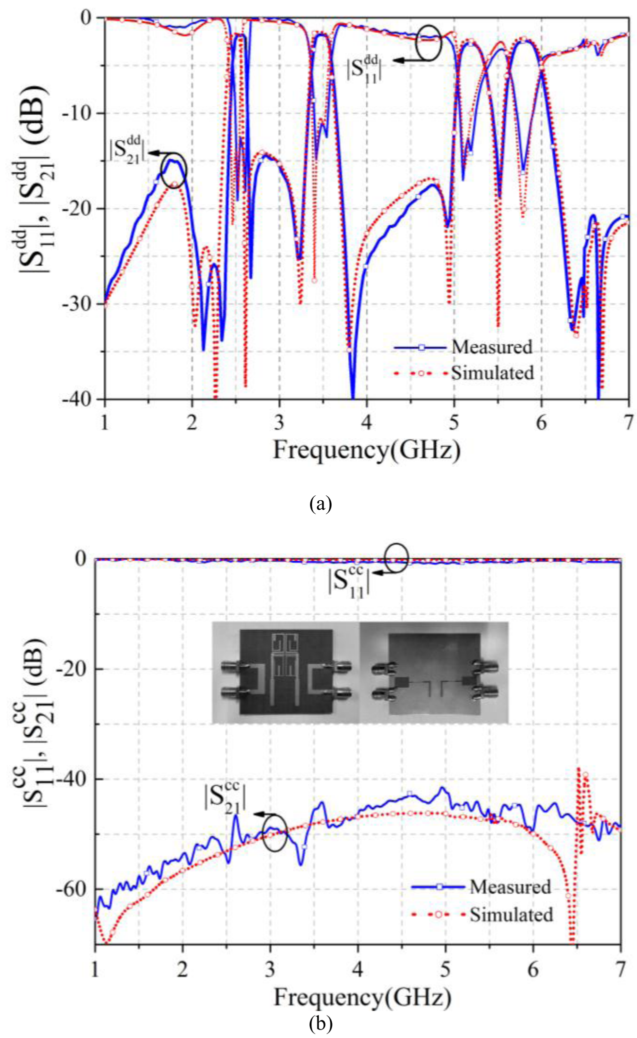

FIGURE 11. Simulated and measured S-parameters of the balanced quad-band BPF under (a) DM and (b) CM operations.

The proposed BPF is measured by Agilent network analyzer N5230A. The effective dimension is only 51.9 mm × 40.4 mm (0.58 λ_g× 0.45 λ_g, where λ_g is the guide wavelength at 2.48 GHz). All the dimensions are selected as follows: $W_{i1} = 2.5$ mm, $W_{i2} = 4.0$ mm, $W_{i3} = 2.5$ mm, $L_{i1} = 14.0$ mm, $L_{i2} = 14.0$ mm, $L_{i3} = 17.0$ mm, $L_{i4} = 17.0$ mm, $W_{s1} = 5.0$ mm, $W_{s2} = 0.6$ mm, $W_{s3} = 0.2$ mm, $W_{s4} = 0.7$ mm, $W_{s5} = 0.2$ mm, $W_{s6} = 0.4$ mm, $W_{s7} = 6.0$ mm, $L_{s1} = 8.0$ mm, $L_{s2} = 4.0$ mm, $L_{s3} = 4.0$ mm, $L_{s4} = 9.35$ mm, $L_{s5} = 5.90$ mm, $L_{s6} = 8.0$ mm, $W_{m1} = 2.4$ mm, $W_{m2} = 1.5$ mm, $W_{m3} = 1.5$ mm, $L_{m1} = 15.0$ mm, $L_{m2} = 14.7$ mm, $W_1 = 0.4$ mm, $W_2 = 0.8$ mm, $W_3 = 0.6$ mm, $W_4 = 1.0$ mm, $L_1 = 14.5$ mm, $L_2 = 16.0$ mm, $L_3 = 5.6$ mm, $L_4 = 9.0$ mm, $L_5 = 15.6$ mm, $L_6 = 3.4$ mm, $L_p = 5.925$ mm, $W_{p1} = 0.5$ mm, $p_1 = 0.15$ mm, $p_2 = 0.1$ mm, $g_1 = 0.125$ mm, $g_2 = 0.2$ mm, $g_3 = 0.15$ mm, $g_4 = 6.0$ mm, $g_5 = 1.2$ mm, $g_6 = 0.6$ mm.

Fig. 11 depicts the simulated and measured results of the BPF. The measured center frequencies are 2.48/ 3.45/ 5.17 /

TABLE 1. Comparison with some recently reported balanced multi-band BPFS.

	f_0 (GHz)	*IL (dB)*	*Con. f_0*	*Number of TZs*	$\frac{\Delta_{3dB}}{\Delta_{20dB}}$	*CMS. (dB)*	*Circuit size (λg^2)*
Ref. [8]	2.5/3.5/5.8	0.8/2.3/2.4	Yes	2	0.39/0.22/0.10	31	0.38×0.18
Ref. [11]	1.54/2.45/3.58/5.2	1.9/2.8/3.7/4.6	Yes	5	0.28/0.28/0.27/0.37	32	0.45×0.32
This Work	**2.48/3.45/5.17/5.78**	**1.74/1.73/2.48/2.35**	**Yes**	**8**	**0.53/0.50/0.59/0.53**	**42**	**0.58 × 0.45**

IL= Insertion loss; Con. = Controllable; CMS. = Common-mode Suppression

5.78 GHz with the 3 dB bandwidths are 149/ 225/ 310/ 400 MHZ (5.96% /6.43% /5.96% /6.90%). The minimum insertion losses are 1.74 /1.73/ 2.48/ 2.35 dB and the return losses are better than 12.0 dB. Eight TZs are obtained and located at 2.03, 2.27, 2.61, 3.24, 3.79, 4.94, 5.50 and 6.39 GHz, respectively, which contributes to a higher selectivity. The CM suppression is better than 42.0 dB within all the DM passbands. A comparison of the performance of the proposed BPF with other balanced multi-band ones is shown in Table 1. It can be seen that the proposed BPF outperforms the others in terms of the DM/CM responses.

IV. CONCLUSION

In this paper, a balanced quad-band balanced BPF is presented by employing two FASLRs. A novel interdigital coupled line is proposed to further improve the selectivity of the BPF. The proposed BPF can achieve controllable DM center frequencies, high CM suppression and sharp passband roll-off skirts. The measured results of the fabricated balanced BPF centered at 2.48/3.45/5.17/5.78 GHz agree well with the simulated ones, which validates the proposed design method well. Therefore, the proposed balanced quad-band BPF has a good potential to be utilized in the applications for balanced multi-band communication systems.

REFERENCES

[1] W. Feng, L. Gu, W. Che, and H. Chen, "Tri-band microstrip bandpass filter using input/output cross coupling," *Int. J. Electron.*, vol. 101, no. 3, pp. 405–409, 2014.

[2] J. Xu, W. Wu, and G. Wei, "Compact multi-band bandpass filters with mixed electric and magnetic coupling using multiple-mode resonator," *IEEE Trans. Microw. Theory Techn.*, vol. 63, no. 12, pp. 3909–3919, Dec. 2015.

[3] L. Gao, X. Y. Zhang, X.-L. Zhao, Y. Zhang, and J.-X. Xu, "Novel compact quad-band bandpass filter with controllable frequencies and bandwidths," *IEEE Microw. Wireless Compon. Lett.*, vol. 26, no. 6, pp. 395–397, Jun. 2016.

[4] J. Wang, S. He, and D. Gan, "A 2.4/3.5/5.2/5.8-GHz quad-band BPF using SLRs and triangular loop resonators," *Electron. Lett.*, vol. 54, no. 5, pp. 299–301, 2018.

[5] Q. Yang, Y.-C. Jiao, and Z. Zhang, "Compact multiband bandpass filter using low-pass filter combined with open stub-loaded shorted stub," *IEEE Trans. Microw. Theory Techn.*, vol. 66, no. 4, pp. 1926–1938, Apr. 2018.

[6] J. Ai, Y. Zhang, K. D. Xu, D. Li, and Y. Fan, "Miniaturized quint-band bandpass filter based on multi-mode resonator and λ/4 resonators with mixed electric and magnetic coupling," *IEEE Microw. Wireless Compon. Lett.*, vol. 26, no. 5, pp. 343–345, May 2016.

[7] J. Shi and Q. Xue, "Novel balanced dual-band bandpass filter using coupled stepped-impedance resonators," *IEEE Microw. Wireless Compon. Lett.*, vol. 20, no. 1, pp. 19–21, Jan. 2010.

[8] F. Wei, Y. J. Guo, P. Y. Qin, and X. W. Shi, "Compact balanced dual- and tri-band bandpass filters based on stub loaded resonators," *IEEE Microw. Wireless Compon. Lett.*, vol. 25, no. 2, pp. 76–78, Feb. 2015.

[9] J.-X. Chen, J. Li, and J. Shi, "Miniaturized dual-band differential filter using dual-mode dielectric resonator," *IEEE Microw. Wireless Compon. Lett.*, vol. 28, no. 8, pp. 657–659, Aug. 2018.

[10] F. Bagci, A. Fernández-Prieto, A. Lujambio, J. Martel, J. Bernal, and F. Medina, "Compact balanced dual-band bandpass filter based on modified coupled-embedded resonators," *IEEE Microw. Wireless Compon. Lett.*, vol. 27, no. 1, pp. 31–33, Jan. 2017.

[11] S.-X. Zhang, L.-L. Qiu, and Q.-X. Chu, "Multiband balanced filters with controllable bandwidths based on slotline coupling feed," *IEEE Microw. Wireless Compon. Lett.*, vol. 27, no. 11, pp. 974–976, Nov. 2017.

[12] X. Guo, L. Zhu, and W. Wu, "Strip-loaded slotline resonators for differential wideband bandpass filters with intrinsic common-mode rejection," *IEEE Trans. Microw. Theory Techn.*, vol. 64, no. 5, pp. 450–458, Feb. 2016.

[13] P. Geng, S. Yang, Z.-X. Xu, and T. Chen, "Compact tri-mode microstrip filter with wide-stopband using asymmetric stub loaded resonators," in *Proc. IEEE MTT-S Int. Microw. Workshop Ser. Adv. Mater. Processes Rf Thz Appl.*, Jul. 2016, pp. 1–3.

[14] H. Shaman and J. S. Hong, "Asymmetric parallel-coupled lines for notch implementation in UWB filters," *IEEE Microw. Wireless Compon. Lett.*, vol. 17, no. 7, pp. 516–518, Jul. 2007.

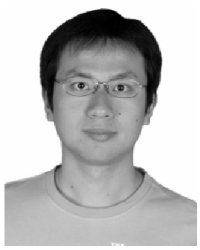

FENG WEI was born in Shaanxi, China, in 1978. He received the B.Eng., M.Eng., and Ph.D. degrees in electrical engineering from Xidian University, Xi'an, China, in 2001, 2004, and 2009, respectively. From 2004 to 2006, he was a RF Engineer with ZTE Corporation. From 2013 to 2014, he was a Visiting Scholar with the Commonwealth Scientific and Industrial Research Organisation (CSIRO), Australia. Since 2009, he has been with the Collaborative Innovation Center of Information Sensing and Understanding, Xidian University, and the National Key Laboratory of Antennas and Microwave Technology, Xidian University, as a Lecturer and an Associate Professor. He has authored or coauthored over 60 international and regional refereed journal papers. His recent research interests mainly include the design of microwave components, circuits, and RFID systems. He is a senior Member of CIE. He has served as a Reviewer for the IEEE Transactions on Microwave Theory and Techniques and the IEEE Microwave and Wireless Components Letters.

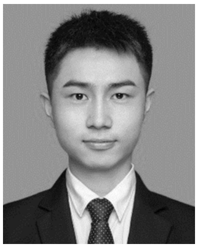

HAO JIE YUE was born in Shaanxi, China, in 1995. He received the B.Eng. degree from the School of Electronic Engineering, Xidian University, Xi'an, China, in 2017, where he is currently pursuing the master's degree in antenna and microwave. His recent research interest includes mainly in the design of balanced passive device.

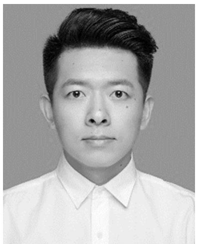

XIAO HANG ZHANG was born in Shanxi, China, in 1994. He received the B.Eng. degree from the School of Electronic Engineering, Xidian University, Xi'an, China, in 2017, where he is currently pursuing the master's degree in antenna and microwave.

XIAO-WEI SHI received the B.Sc. degree in radio physics, and the M.Eng. and Ph.D. degrees in electrical engineering from Xidian University, Xi'an, China, in 1982, 1990, and 1995, respectively, where he has been with the National Key Laboratory of Antennas and Microwave Technology, as a Lecturer, an Associate Professor, and a Professor, since 1990. He is also the Director of Office for Science & Technology, Xidian University. He was a Postdoctoral Fellow with the Electronics and Telecommunications Research Institute (ETRI), South Korea, from 1996 to 1997. He has published over 50 international and regional refereed journal papers. His recent research interests mainly include smart antennas design, electromagnetic inverse scattering, and electromagnetic compatibility. He received the first-class Prize of Excellent Teaching of Shaanxi Province, in 1995, and Scientific Progress Awards of Shaanxi Province, in 1992.